

Nonsequential Double Ionization with Polarization-gated Pulses

W. Quan and X. Liu

State Key Laboratory of Magnetic Resonance and Atomic and Molecular Physics, Wuhan Institute of Physics and Mathematics, Chinese Academy of Sciences, Wuhan 430071, P. R. China

C Figueira de Morisson Faria

Department of Physics and Astronomy, University College London, Gower Street, London WC1E 6BT, United Kingdom

Abstract. We investigate laser-induced nonsequential double ionization by a polarization-gated laser pulse, constructed employing two counter-rotating circularly polarized few cycle pulses with a time delay T_d . We address the problem within a classical framework, and mimic the behavior of the quantum-mechanical electronic wave packet by means of an ensemble of classical electron trajectories. These trajectories are initially weighted with the quasi-static tunneling rate, and with suitably chosen distributions for the momentum components parallel and perpendicular to the laser-field polarization, in the temporal region for which it is nearly linearly polarized. We show that, if the time delay T_d is of the order of the pulse length, the electron-momentum distributions, as functions of the parallel momentum components, are highly asymmetric and dependent on the carrier-envelope (CE) phase. As this delay is decreased, this asymmetry gradually vanishes. We explain this behavior in terms of the available phase space, the quasi-static tunneling rate and the recollision rate for the first electron, for different sets of trajectories. Our results show that polarization-gating technique may provide an efficient way to study the NSDI dynamics in the single-cycle limit, without employing few-cycle pulses.

1. Introduction

Polarization gating, since being proposed in the mid 1990s [1], has turned into a powerful tool for attosecond metrology, and dynamic imaging of matter [2], mainly due to its simplicity and reliability. The key idea behind it is to combine laser fields of different polarizations and sometimes frequencies in such a way as to obtain controllable, near-linearly polarized, extremely short driving laser pulses. An important application of this technique is, for instance, the generation of isolated attosecond pulses [3, 4, 5], some of them as short as 130 attoseconds [6]. The latter pulses have been accomplished by employing, as a driving field, a left circularly polarized and a time-delayed right circularly polarized sub-10fs laser pulse. The resulting driving pulse changes from circularly polarized to almost linearly polarized, and then back to circularly polarized, within the pulse envelope.

The importance of these drastic ellipticity changes is a consequence of the physical mechanism behind high-order harmonic generation (HHG). This phenomenon, which is employed in the generation of attosecond pulses, is the result of a three-step physical process [7]. Thereby, the valence electron of an atom, subjected to an intense laser field, is released in the continuum by tunnel ionization. This electron is then accelerated by the field and, depending on its energy, ionization time and on the laser-field polarization, it may be driven back towards its parent ion and recombine at a later instant. Upon recombination, the energy acquired by the electron from the field is released as a high-frequency photon. Gating is important, as it may be employed to restrict the electron ionization and recombination times to very narrow intervals. If the field is circularly polarized, the returning electron will miss the atomic core, whereas, if the field is linearly polarized, the electron will interact with it.

Laser-induced nonsequential double ionization (NSDI) is also caused by a similar mechanism. The main difference lies on the fact that the returning electron, instead of recombining with a bound state of its parent ion, will rescatter inelastically with it, giving part of its kinetic energy to release a second electron. This nonsequential physical mechanism has been revealed by very peculiar features in the electron momentum distributions, namely symmetric peaks at the nonvanishing momenta $p_{1\parallel} = p_{2\parallel} = \pm 2\sqrt{U_p}$, where U_p denotes the ponderomotive energy and $p_{n\parallel}$ ($n = 1, 2$) the electron momentum components parallel to the laser field polarization [8]. Therefore, we expect that NSDI may also be strongly influenced by the time dependence of the external laser field, for example, by the dramatic change of its amplitude and polarization. This is supported by our previous work on NSDI with few-cycle, linearly polarized driving pulses [9, 10, 11]. Therein, we have shown, both theoretically [10, 11] and experimentally [9], that the NSDI dynamics are strongly dependent on the carrier-envelope (CE) phase. Indeed, we observed strongly asymmetric distributions, which would shift from the positive to the negative region, or vice versa, of the plane $(p_{1\parallel}, p_{2\parallel})$ spanned by the electron momentum components $p_{n\parallel}$ ($n = 1, 2$) parallel to the laser-field polarization, as the CE phase was changed. Furthermore, it has been shown, for NSDI with a single elliptically polarized driving field, that the electron-momentum distributions are highly dependent on the driving-field polarization [12].

Hence, one can raise the question of whether polarization gating may be used to control NSDI dynamics. This issue is of interest for two main reasons. Firstly, since one may build an extremely short, almost linearly polarized driving field, it may be possible to steer the electron motion with a much higher precision than with,

for instance, linearly polarized few-cycle pulses. Secondly, sometimes the changes observed in the NSDI electron momentum distributions, with regard to the driving-field shape, are far more dramatic than in high-order harmonic or above-threshold ionization spectra. This is due to the fact that different sets of electron orbits may be mapped into different momentum regions. Apart from that, if the second electron is dislodged by electron-impact ionization, there will be a minimum and a maximum parallel momentum for which this process is classically allowed. Depending on the field parameters, we can employ this particular feature to make whole momentum regions appear or collapse. The above-stated effects have been observed for NSDI with linearly polarized few cycle pulses, and led to dramatic changes in the electron momentum distributions [9, 10, 11].

In this work, we investigate differential electron momentum distributions in NSDI with polarization gating. For that purpose, we extend the classical model employed in our previous publications [10, 11] to the elliptical-polarization case. In this model, the quantum-mechanical transition probability corresponding to the scenario in which the second electron is released by electron-impact ionization, within the strong-field approximation, is mimicked by a classical ensemble of electrons released in the continuum with a quasi-static tunneling rate [10, 11, 13]. The main difference is that, for elliptically polarized fields, one must take into account that the lateral residual laser electric field influences the electron orbits in the continuum, and also at the instant of ionization. As the external driving field, we consider the same pulse configuration as in [5], i.e., two counter-rotating, time-delayed circularly polarized few-cycle pulses. We investigate the influence of both the CE phase and of the delay between the two pulses on the electron momentum distributions. In a more general context, it is worth mentioning that classical models have proven to be very powerful in the context of nonsequential double [14] or multiple [15] ionization.

This paper is organized as follows. In Sec. 2, we provide a brief discussion of our model, placing a particular emphasis on how it differs from its counterpart for linearly polarized fields. Subsequently (Sec. 3), we present the differential electron momentum distributions, and analyze their main features in terms of electron trajectories. Finally, our conclusions and a summary of this work are given in Sec. 4.

2. Model

We consider an electron ensemble subject to a pulse with a time-dependent ellipticity, which is generated by the superposition of a left-circularly polarized pulse, and right-circularly polarized pulse. The two pulses are taken to be identical except by their polarization, and there is a time delay T_d between them. Below, we provide more details about the pulse shape, and our classical ensemble model, which is employed to imitate the behavior of a quantum-mechanical wave packet. Atomic units are being used throughout.

2.1. Polarization-gated driving field

Explicitly, the electric fields $\vec{E}_l(t)$ and $\vec{E}_r(t)$ of the left- and right circularly polarized pulses read

$$\vec{E}_l(t) = E_0 e^{-2 \ln(2)((t-T_d/2)/\tau_p)^2} [\hat{x} \cos(\omega(t - T_d/2) + \phi) + \hat{y} \sin(\omega(t - T_d/2) + \phi)] \quad (1)$$

$$\begin{aligned} \vec{E}_r(t) = E_0 e^{-2 \ln(2)((t+T_d/2)/\tau_p)^2} \\ [\hat{x} \cos(\omega(t + T_d/2) + \phi) - \hat{y} \sin(\omega(t + T_d/2) + \phi)], \end{aligned} \quad (2)$$

respectively. In the above-stated equations, E_0 is the peak-field amplitude, ω is the carrier frequency, τ_p is the pulse duration, T_d is the time delay between the two circularly polarized pulses and ϕ is CE phase. The unit vectors in the x and y directions are denoted by \hat{x} and \hat{y} .

The electric field components of the combined laser pulse in the x and y direction are given by

$$\begin{aligned} \vec{E}_x(t) = E_0 e^{-2 \ln(2)((t-T_d/2)/\tau_p)^2} [\cos(\omega(t - T_d/2) + \phi)] \\ + E_0 e^{-2 \ln(2)((t+T_d/2)/\tau_p)^2} [\cos(\omega(t + T_d/2) + \phi)] \end{aligned} \quad (3)$$

and

$$\begin{aligned} \vec{E}_y(t) = E_0 e^{-2 \ln(2)((t-T_d/2)/\tau_p)^2} [\sin(\omega(t - T_d/2) + \phi)] \\ - E_0 e^{-2 \ln(2)((t+T_d/2)/\tau_p)^2} [\sin(\omega(t + T_d/2) + \phi)], \end{aligned} \quad (4)$$

respectively. The time-dependent ellipticity of this pulse is

$$\xi(t) = \frac{|1 - \exp[-4 \ln(2)tT_d/\tau_p^2]|}{1 + \exp[-4 \ln(2)tT_d/\tau_p^2]}. \quad (5)$$

In the vicinity of $t = 0$, $\xi(t)$ increases from 0 to 0.2 and is approximately linear. Outside this interval, this approximation does not hold. The temporal region for which the field polarization is approximately linear is known as the “polarization gate” [1].

In Ref. [5], the polarization gate for the specific laser-field configuration discussed above has been estimated to be around $0.3\tau_p$. Therein, it has also been shown that it is inversely proportional to the time delay T_d between the two pulses. Hence, to reduce the polarization gate, we can either use shorter circularly polarized pulses or increase T_d . From the experimental perspective, either of them can be controlled at will. In fact, the length of the laser pulse will be conditioned by state-of-the-art ultrafast laser technique [16]. However, the delay time between the two circularly polarized laser pulses cannot be too long. If we use a too long delay between the two circularly polarized laser pulses, to obtain a sufficiently intense combined pulse it may be necessary to strengthen our laser pulses so much that the ground-state sample may be depleted and result in a poor signal-to-noise ratio.

2.2. Electron momentum distributions

We will now discuss how we mimic the quantum-mechanical electron momentum distributions in a classical framework. Similar models have been employed in [10, 11, 13] for linearly polarized fields. We consider a set of classical trajectories, starting at different tunneling times t_0 throughout the pulse. We limit such times to the time interval for which the field is almost linearly polarized. This is justified, as, only in this time range, a significant contribution to NSDI will occur. Furthermore, in the specific model discussed in this paper, we make three main assumptions. First, each trajectory is weighted with the tunneling probability per unit time given by the well-known quasi-static formula [17]

$$W_t(t_0) \sim \frac{1}{|E_{\text{sum}}(t_0)|} \exp \left[\frac{-2(2|E_{IP1}|)^{3/2}}{3|E_{\text{sum}}(t_0)|} \right], \quad (6)$$

where E_{IP1} is the first ionization threshold of the atom in question, and $\vec{E}_{\text{sum}}(t_0) = \vec{E}_x(t_0) + \vec{E}_y(t_0)$ is the electric field of the combined, polarization-gated laser pulse. Second, to simulate the initial wave-packet spreading, an initial lateral velocity v_l is further introduced. Each trajectory is then weighted with the tunneling probability times the quantum-mechanical transverse velocity distribution weight [18], W_l , which can be calculated by

$$W_l(v_l) = \frac{1}{\pi(\delta v_l)^2} \exp[-(\frac{v_l}{\delta v_l})^2], \quad (7)$$

where the lateral velocity width is given by

$$\delta v_l = (E_{\text{sum}}/\sqrt{2E_{IP1}})^{1/2}. \quad (8)$$

The range for the transverse velocity distribution chosen here is $2\delta v_l$. Finally, a quantum-mechanical wave packet also spreads in time, so that the contributions of the longer orbits are weakened. We incorporate this final ingredient in a similar way as in Ref. [12], by introducing an extra weight $(t_1 - t_0)^{-3}$ to each electron trajectory. Thereby, t_1 denotes the time the electron returned to the core. Therefore, the overall weight of each trajectory in the ensemble reads

$$W_k(t_0, v_l) = W_t(t_0) \times W_l(v_l) \times (t - t_0)^{-3}. \quad (9)$$

After tunneling, the equations of motion for the electron in both directions are

$$\ddot{x} = \vec{E}_x(t) \quad (10)$$

$$\ddot{y} = \vec{E}_y(t). \quad (11)$$

In order to obtain the electron orbits, Eq. (10) and Eq. (11) are integrated, and the Coulomb potential is ignored. This is a reasonable assumption for a strong driving field. Electrons are assumed to be ‘born’ at time t_0 at the origin $x = 0, y = 0$ with initial lateral velocity. Only those electrons coming back to the core with energy larger than E_{IP2} , the second ionization threshold of the atom, will contribute to the NSDI yield. This corresponds to the physical situation in which the first electron dislodges the second by electron-impact ionization. After a trajectory is launched, by checking the position of the electron, we determine whether it has returned to the core, and, if so, its return time. The electron velocities in both directions, \dot{x} and \dot{y} , are then evaluated. The energy of the electron, upon return, is

$$E_{\text{ret}} = \frac{1}{2}(\dot{x}^2 + \dot{y}^2). \quad (12)$$

If the condition $E_{\text{ret}} > E_{IP2}$ is satisfied [13], the first electron gives part of its kinetic energy E_{ret} upon return to a second electron, so that it is able to overcome the second ionization threshold E_{IP2} . The electron pair then obeys

$$\begin{aligned} \frac{1}{2} \sum_{j=1}^2 [p_{jx} + A_x(t_1)]^2 &= E_{\text{ret}} - E_{IP2} - \frac{1}{2} \sum_{j=1}^2 p_{jz}^2 \\ &\quad - \frac{1}{2} \sum_{j=1}^2 [p_{jy} + A_y(t_1)]^2. \end{aligned} \quad (13)$$

In Eq. (13), $A_x(t)$ and $A_y(t)$ denote the vector potential-components

$$A_x(t) = - \int E_x(t) dt \quad (14)$$

$$A_y(t) = - \int E_y(t) dt \quad (15)$$

of the laser pulse in the x and y directions, and p_{jx} , p_{jy} and p_{jz} are the final momentum components recorded by the detector in the x , y and z direction after tunneling.

One should note that the energy-conservation condition (Eq. (13)) gives the equation of a hypersphere in the six-dimensional space spanned by the momentum components of the two electrons. This hypersphere exhibits the radius $[2(E_{\text{ret}}(t_1) - E_{IP2})]^{1/2}$ and is centered at $(p_{1x}, p_{1y}, p_{1z}; p_{2x}, p_{2y}, p_{2z}) = (-A_x(t_1), -A_y(t_1), 0; -A_x(t_1), -A_y(t_1), 0)$. Therefore, the larger the electron kinetic energy is, the larger is the region for which electron-impact ionization is classically allowed. Furthermore, the above-stated equation shows that the distributions should be centered at nonvanishing electron momenta. Specifically for monochromatic, linearly polarized fields, the vector potential upon return can be approximated by $2\sqrt{U_p}$. This corresponds to the situation in which the electron leaves at a field maximum and returns at a crossing. Since this is the most probable momentum for the electron upon return, we expect the distributions to be centered at this quantity. We have observed, however, for the parameters employed in this work, that this estimate roughly holds.

The electron momentum distributions then read

$$R \sim \int \int dt_0 dv_l W_k(t_0, v_l) \delta(E_{\text{ret}}(t_1) - E_{IP2} - \sum_{j=1}^2 \frac{[p_{jx} + A_x(t_1)]^2}{2} - \sum_{j=1}^2 \frac{[p_{jy} + A_y(t_1)]^2}{2} - \sum_{j=1}^2 \frac{p_{jz}^2}{2}). \quad (16)$$

The argument of the δ function gives the energy-conservation restriction. Since the situation addressed in this paper occurs only in the xy plane, the electron motion in the z direction is ignored.

In Eq. (16), there is also an additional assumption, namely that the second electron is released by a contact-type interaction placed at the position of the ion. In this case, the electron momentum distributions are mainly determined by the momentum-space integration. This means that they are isotropic in momentum space, have the radius of the above-mentioned hypersphere, and are centered at the most probable momentum upon return. This guarantees that we investigate only the effects of the gating on the NSDI momentum distributions. Other types of electron-electron interaction would lead to a term $|V_{\mathbf{p}_n, \mathbf{k}}|^2$ dependent on the final momenta \mathbf{p}_n ($n = 1, 2$), and on the intermediate momentum \mathbf{k} in the above distributions (for details see Ref. [13]). Such extra momentum dependence might distort or mask the effects of the polarization gating.

3. Results

In this section, we display the NSDI electron-momentum distributions computed with Eq. (16) and the polarization-gated pulse described in Sec. 2.1. This pulse has been chosen as the superposition of two time-delayed, circularly polarized pulses of wavelength $\lambda = 800$ nm. The full width at half maximum (FWHM) of the circularly

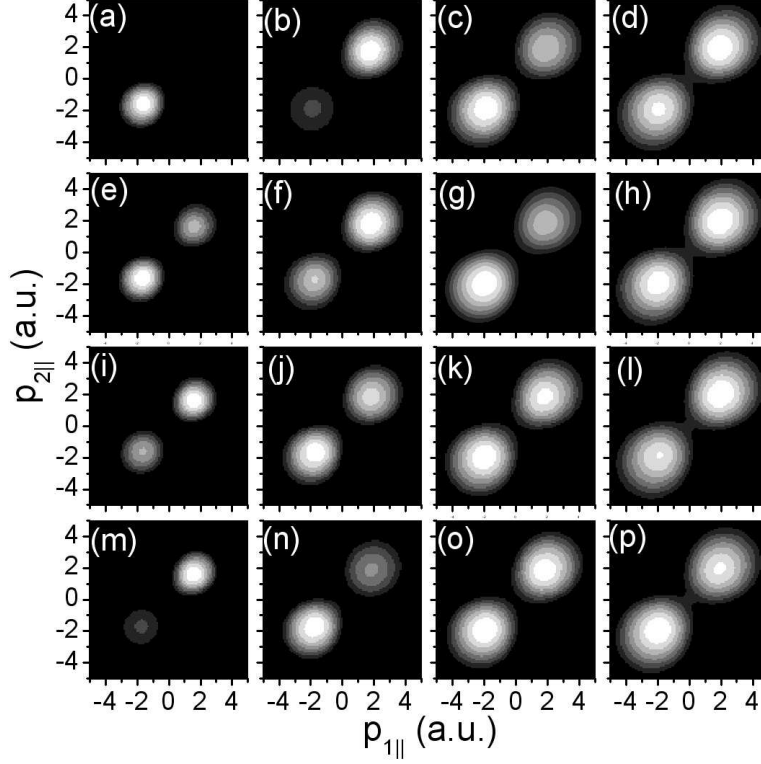


Figure 1. NSDI electron momentum distributions computed for Neon in a polarization-gated pulse described by Eqs. (3)-(4). The peak intensity of the two circularly polarized pulses is $2 \times 10^{14} \text{W/cm}^2$, their length is four cycles ($n = 4$) and their frequency is $\omega = 0.057 \text{ a.u.}$ The distributions are plotted as functions of the momentum components $p_{n||}$ ($n = 1, 2$) parallel to the nearly linearly polarized part of the combined pulse. The CE phase is varied from the top to the bottom of the figure, and the delay ωT_d between the two pulses from its left to its right. In the first, second, third and fourth rows from the top [panels (a) to (d), panels (e) to (h), panels (i) to (l), and (m) to (p), respectively], the CE phases ϕ are 0.5π , 0.8π , 1.0π , and 1.2π respectively. In the first [panels (a), (e), (i) and (m)], second [panels (b), (f), (j) and (n)], third [panels (c), (g), (k) and (o)], and fourth [panels (d), (h), (l) and (p)] columns from the left, we depict distributions for the delay phases $\omega T_d = 8\pi$, 6π , 4π , and 2π .

polarized light is chosen as four cycles, i.e., $\tau \sim 10 \text{ fs}$. The distributions were calculated for neon. For this specific species, the dominant physical mechanism is electron-impact ionization. For other species, such as argon, the excitation of the parent ion by the returning electron, with subsequent double ionization, plays an important role [8, 19].

Such distributions are depicted in Figure 1, as functions of the electron momentum components parallel to the laser-field polarization at the very center of the gate. For the pulse shape considered in this paper, this corresponds to the x direction. Unless otherwise stated (see, e.g., Figs. 5 and 6), we will denote such momentum components

as $p_{n\parallel}$ ($n = 1, 2$). One should note, however, that, in the calculations, the electron is propagated in both x and y directions.

If the delay phase between both pulses is equal to the pulse length, i.e., $\omega T_d = 8\pi$, the distributions are, in general, highly asymmetric and concentrated either in the positive or the negative parallel momentum regions. For the specific parameters in this work, as the CE phase ϕ is changed from $\phi = 0.5\pi$ to $\phi = 1.2\pi$, the distributions shift from the third to the first quadrant of the plane $(p_{1\parallel}, p_{2\parallel})$ spanned by the parallel-momentum components. This behavior is shown in the far left panels of Fig. 1, i.e., in Figs. 1(a), 1(e), 1(i), and 1(m), and resembles to a great extent what happens for linearly polarized few-cycle pulses.

In this latter case, we have shown that the asymmetry and the shifts in the distributions were due to the changes in the dominant set of trajectories along which the first electron would return. This set of trajectories strongly depends on the CE phase, so that the asymmetry can be used to determine this parameter [10, 11]. The behavior of the electron-momentum distributions in the present case suggests a similar physical interpretation. From the positions of maxima, at approximately $(2\sqrt{U_p}, 2\sqrt{U_p})$ and $(-2\sqrt{U_p}, -2\sqrt{U_p})$, we verify that the estimates for the peaks of the distributions, for monochromatic, linearly polarized fields, roughly holds in this case.

As the delay phase is reduced to $\omega T_d = 6\pi$, the distributions become wider and the electron yield becomes much higher. This is shown in the second column of Fig. 1 [Figs. 1(b), 1(f), 1(j) and 1(n)]. The increase in width suggests that the radius of the hypersphere (13), which delimits the classically allowed region, increased. Physically, this would correspond to a larger kinetic energy $E_{\text{ret}}(t_1)$ of the first electron upon return. The growth in electron yield hints at an increase in the tunneling probability for the first electron. The distributions, however, exhibit a similar qualitative behavior to that observed for $\omega T_d = 8\pi$, in the sense that they are asymmetric and depend on the CE phase.

A closer inspection, however, reveals a dramatic change, in the sense that the electron distributions are concentrated in an opposite momentum region, as compared to their counterparts at the delay phase of 8π . For example, if the CE phase is 0.5π , such distributions are almost entirely localized in the first quadrant of the parallel momentum plane for $\omega T_d = 6\pi$ [Fig. 1(b)], while, for $\omega T_d = 8\pi$, they occupy the negative momentum region [Fig. 1(a)]. This sharp contrast persists for the other values of CE phases. The reason behind this shift will be addressed later.

If the delay between both pulses is decreased further, the overall asymmetry in the electron momentum distributions starts to fade. This may be seen in the third column of Fig. 1 [Figs. 1(c), 1(g), 1(k) and 1(o)], for which $\omega T_d = 4\pi$. Such distributions are only slightly asymmetric and exhibit bright spots both in the first and third quadrants of the $(p_{1\parallel}, p_{2\parallel})$ plane. This trend persists for an even shorter delay of $\omega T_d = 2\pi$, as shown in the far right panels of Fig. 1 [Figs. 1(d), 1(f), 1(l), and 1(p)]. In this latter case, the distributions are nearly symmetric and the information about the CE phase is almost lost.

This result is rather counterintuitive, as it resembles more the distributions obtained for a linearly monochromatic driving field than what is expected for a combination of two few-cycle pulses. In the former case, the distributions are totally symmetric upon $(p_{1\parallel}, p_{2\parallel}) \rightarrow (-p_{1\parallel}, -p_{2\parallel})$. In our previous work [10], we observe that this symmetry holds in practice if the pulse is longer than 10 cycles. However, the longest quasi-linearly polarized pulse considered here has no more than 4 cycles, as the

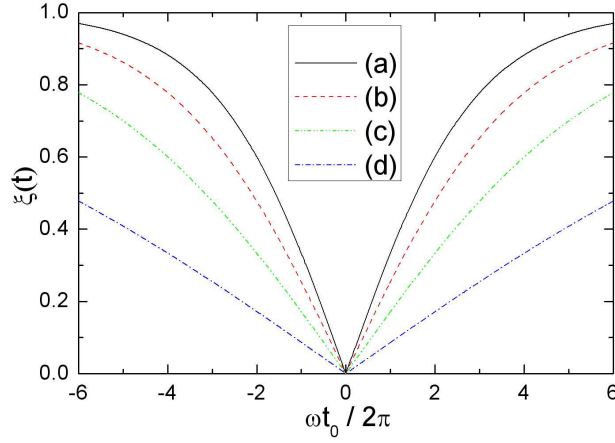


Figure 2. The ellipticity of the combined field \vec{E}_{sum} , close to the center of the polarization gate, as a function of the electric field initial phase ωt_0 . The CE phase of the laser field is chosen as 0.5π , while the delay phases are 8π , 6π , 4π and 2π (tags (a), (b), (c) and (d), respectively). The remaining parameters are the same as in the previous figure.

gate width must be less than the laser-pulse duration. Therefore, intuitively, one would anticipate asymmetric distributions. In the following, we will give an explanation for such a surprising result based on lateral electron dynamics.

For that purpose, we will have a closer look at how the ellipticity of the combined laser field varies, with respect to the delay phase ωT_d . These results are displayed in Fig. 2, and show that the delay phase ωT_d has a strong influence on the ellipticity of the very-center portion of the combined laser field. A longer delay phase corresponds to a sharper slope. When $\omega T_d = 8\pi$, the ellipticity drops very steeply to zero around $\omega t_0 = 0$ and changes back soon after that. Hence, for longer time delays T_d , the start times t_0 of the first electron are restricted to a very narrow interval and the gate behaves better. This sheds some light on why the results in the first column in Fig. 1, computed for 8π delay phase, are similar to those obtained with linearly polarized driving fields. In contrast, we have verified that variations in the CE phase do not change the ellipticity of the combined laser field.

In Fig. 3, we analyze the behavior of the ionization rate for the first electron and the phase-space contributions with respect to delay phase ωT_d . We consider parallel momenta along the diagonal, i.e., $p_{1\parallel} = p_{2\parallel} = p_{\parallel}$, and impose that the perpendicular momentum components vanish. The classically allowed momentum region is most extensive for vanishing transverse momenta. Hence, we expect that the figure will provide a rough upper bound for it. We also fix the CE phase at 0.5π . A similar analysis has been performed in Ref. [10] for linearly polarized few-cycle pulses.

In the two upper panels [Fig. 3(i) and Fig. 3(ii), respectively], we display the calculated ADK ionization rate in the central portion of the combined pulse, and the final recollision rate for the first electron. The tabs, (a),(b),(c),(d) in the figure follow those in Fig. 1, i.e., from (a) to (d), the delay phase is varied from 8π to

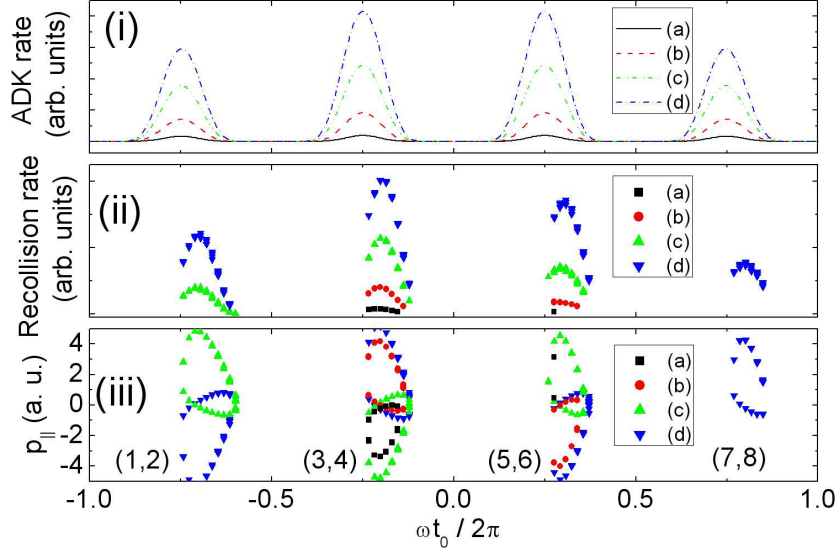


Figure 3. Ionization and recollision rates, together with the final electron momentum along $p_{1||} = p_{2||} = p_{||}$, as functions of the initial phase ωt_0 , for a pulse described by Eqs. (3) and (4), with CE phase $\phi = 0.5\pi$. Panel (i) exhibits the calculated ADK ionization rate. Panel (ii) displays the final recollision rate, calculated with the ADK rate and lateral velocity distribution rate. Panel (iii) gives the final momentum $p_{||}$. The tabs (a),(b),(c),(d) correspond to the delays $\omega T_d = 8\pi, 6\pi, 4\pi$ and 2π , respectively. The numbers (j, ν) in panel (iii) indicate a pair of electron orbits. The remaining parameters are the same as in Fig. 1.

2π . The recollision rate is weighted according to Eq. (7) and Eq. (9) for the initial lateral velocity distribution. The recollision rate is weighted according to Eq. (9) and decided by three factors, i.e., the tunneling ionization rate, the wave packet spread time and the quantum-mechanical transverse velocity distribution weight. Since the lateral electric field of the combined laser pulse will shift the electron wave packet laterally, trajectories with zero initial lateral velocity, which may return to the core in a linearly polarized laser, will miss the core. Only those with a certain initial lateral velocity, which may compensate the displacement induced by the lateral electric field, can return to the core and contribute to the NSDI yield. The effect of the transverse velocity has been demonstrated in HHG by a recent experiment where an elliptical laser pulse was employed [20].

From Eq. (8), one can see that, as compared to the trajectories with vanishing initial lateral velocity, those with a non-vanishing initial lateral velocity have a lower transverse velocity distribution weight, which in turn reduces the final recollision rate. Therefore, the recollision rate will be corrected according to the transverse electron dynamics. Comparing Figs. 3(i) and (ii), one also finds that the highest recollision rate appears slightly later than the peak of the ADK ionization rate. This is a consequence of the fact that the trajectories starting near the peak laser electric field will propagate

with longer times and be affected more by the wave-packet spreading effect. This effect results in the drop of the recollision rate according to a cubic power law with the evolution time $t_1 - t_0$.

The parallel momenta p_{\parallel} in Fig. 3(iii) provide an approximate estimate for the region in momentum space for which electron-impact ionization is classically allowed. The region delimited by such momenta gives a very good idea of the role of phase-space effects: the larger this region is, the more important they are. A small region, on the other hand, means a small radius for the hypersphere in Eq. (16), which, physically, indicates that the second electron may only be dislodged in a small region in momentum space. In Fig. 3(iii), one may identify a few sets of orbits, which lead to parallel momenta either in the positive or negative region. Starting from the left, these orbits are denoted by (1, 2), (3, 4), (5, 6) and (7, 8).

The momentum region to which they contribute depend on the time delay ωT_d . If this delay is an even multiple of the field cycle 2π , i.e., for $\omega T_d = 4\pi$ and $\omega T_d = 8\pi$, there exist at most two sets of orbits, (1, 2) and (5, 6), which yield contributions in the first quadrant of $(p_{1\parallel}, p_{2\parallel})$. These orbits start within $-2\pi < \omega t_0 < -\pi$ and $0 < \omega t_0 < \pi$, respectively. The remaining sets of orbits, starting at $0 < \omega t_0 < \pi/2$ and $3\pi/2 < \omega t_0 < 2\pi$, lead to negative parallel momenta. If ωT_d is an odd multiple of the field cycle, i.e., for $\omega T_d = 6\pi$ and $\omega T_d = 2\pi$, the above-mentioned situation is reversed.

For linearly polarized driving fields, the ADK ionization rate and phase-space effects suffice, in order to determine whether a set of orbits contributes significantly to the electron-momentum distributions. A large rate indicates that the first electron will tunnel with a significant probability per unit time. Furthermore, if this electron returns with sufficient energy to release the second electron over a significant region of momentum space, one expects that the contributions from a specific set of orbits will be prominent [10, 11]. For a polarization-gated pulse, however, we have to take into account the lateral electron dynamics. This information is embedded in the recollision rate depicted in Fig. 3(ii).

We will now analyze the interplay of the above-mentioned issues in the electron momentum distributions. For a delay $\omega T_d = 8\pi$, there is mainly a single set (3, 4) of trajectories for which electron-impact ionization is classically allowed. This set corresponds to $\omega t_0 \sim -\frac{\pi}{2}$ and leads to contributions in the negative momentum region. The contribution from another set (5, 6) of orbits may be ignored due to its small classical allowed region and low recollision rate. For this reason, the distributions are highly asymmetric and concentrated in the third quadrant of the parallel-momentum plane $(p_{1\parallel}, p_{2\parallel})$, in agreement with Fig. 1(a). This very restricted range in the classically allowed region is possibly due to the fact that the ellipticity of the driving field changes very fast. Hence, the first electron only returns to its parent ion within a very narrow temporal region. The tunneling rate is also weak in this case, as it is taken only in the central part of the combined pulse and there is very little overlap between each circularly polarized pulse for this specific delay.

As the delay phase decreases to $\omega T_d = 6\pi$, the situation becomes different. In this case, the orbits (3, 4) lead to $p_{\parallel} > 0$. Hence, the distributions are concentrated in the positive parallel momentum region. Apart from that, there is also a further set (5, 6) of orbits, whose start times lie near $\omega t_0 \sim \frac{\pi}{2}$. The contributions of this latter pair are weaker, and localized in the third quadrant of the plane $(p_{1\parallel}, p_{2\parallel})$. Finally, as an overall feature, there is an increase in the ADK rate and also in the recollision rate for the first electron. This is due to an increase in the overlap between the two

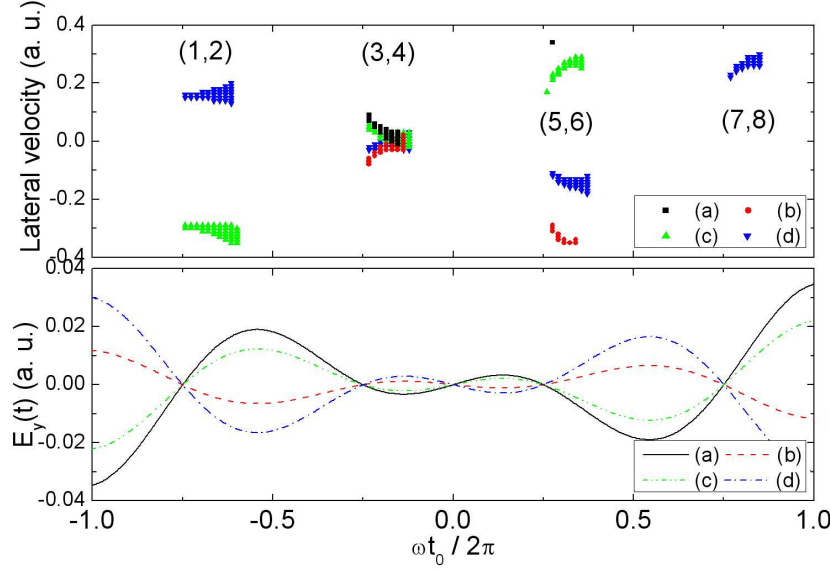


Figure 4. The upper and lower panel show the initial lateral velocities of the rescattering orbits and the lateral laser electric field, respectively, as functions of the laser electric field phase ωt_0 . The tabs, (a),(b),(c),(d), follow those in Fig. 3. The numbers (i, j) in the upper panel denote the orbits composing a pair.

pulses \vec{E}_r and \vec{E}_l , and leads to brighter distributions. All the above-stated features can be observed in Fig. 1(b).

A further reduction in the delay phase to $\omega T_d = 4\pi$ leads to an additional set (7, 8) of orbits for which the first electron may return and release the second electron. This set starts near $\omega t_0 \sim -3\pi/2$, and leads to contributions in the first quadrant of the plane $(p_{1\parallel}, p_{2\parallel})$. This will add up to the contributions from the orbits (5, 6). Hence, overall, there will be two sets of orbits yielding momenta in such a region.

The ionization and recollision rates, however, are larger for the orbits (3, 4) starting at $\omega t_0 \sim -\pi/2$. Therefore, the distributions are slightly brighter in the negative momentum region. Finally, for $\omega T_d = 2\pi$, there are four sets of orbits contributing to the electron-momentum distributions, and the distributions are approximately symmetric.

In Fig. 4, we display the initial lateral velocity for the rescattering orbits (upper panel) and the lateral laser electric field (lower panel), as functions of the initial electric field phase ωt_0 . Classically, for a linearly polarized driving electric field, an electron with a large lateral initial velocity will miss the core. For an elliptically polarized field, however, the lateral electric field will also slightly change the electron's orbit in the transverse direction.

If both effects are combined, a gate can be formed to choose the orbit with a certain initial lateral velocity to come back with highest probability [20]. A larger lateral velocity corresponds to a stronger lateral laser electric field and, according to Eq. (7), to a lower ionization rate. In Fig. 4, the orbits starting near $\omega t_0 \sim -\pi/2$ meet

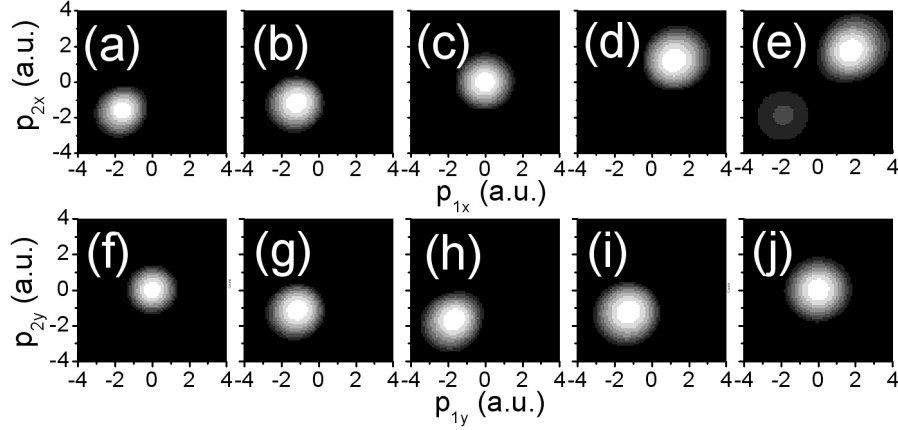


Figure 5. NSDI electron momentum distributions computed for neon in a polarization-gated pulse. The upper and lower panels give the distributions as functions of the momentum components (p_{1x}, p_{2x}) and (p_{1y}, p_{2y}) , respectively. The CE phase is fixed to be 0.5π and the delay phases, from left to right, are 8π [panels (a) and (f)], 7.5π [panels (b) and (g)], 7π [panels (c) and (h)], 6.5π [panels (d) and (i)] and 6π [panels (e) and (j)]. The remaining parameters are the same as in Fig. 1.

the smallest lateral laser electric field because their tunneling phases are those nearest to the center of the gate. Hence, these orbits exhibit the largest recollision probability. This explains why we observe a favored NSDI rate in this region in Fig. 3.

It is also noteworthy that this specific set of orbits exhibits lateral velocities close to zero, whereas the lateral velocities of the remaining sets vary considerably with the time delay. In general, as the delay phase ωT_d decreases, the lateral velocities diminish as well. This causes an overall increase in the tunneling and recollision rates, in agreement with Fig. 3.

Apart from that, specifically for the time delay $\omega T_d = 2\pi$, there is an overall decrease in the lateral velocities for the orbits starting near $\omega t_0 \sim -\pi$ and $\omega t_0 \sim \pi$. Both sets of orbits lead to positive final momenta $p_{n\parallel}$ ($n = 1, 2$). Thus, we will expect an increase in brightness in the first quadrant of the $(p_{1\parallel}, p_{2\parallel})$ plane. As a direct consequence, the distributions are nearly symmetric. The set of orbits (7, 8), starting near $\omega t_0 = 1.5\pi$, exhibit very large transverse velocities and therefore does not contribute significantly to the yield.

Still, one remaining question is how to understand the dramatic change in the electron momentum distributions between the delay phase of 8π and 6π , as shown in Fig. 1. For that purpose, we further conduct the calculations for the CE phase $\phi = 0.5\pi$ and several delay phases between 8π and 6π , i.e., $\omega T_d = 7.5\pi, 7\pi$ and 6.5π . The results are displayed in Fig. 5. In addition to the momentum components (p_{1x}, p_{2x}) in the x direction, we also consider the momentum components (p_{1y}, p_{2y}) . The distributions as functions of the former or latter momentum components are displayed in the upper and lower panels of the figure, respectively. Therefore, for the

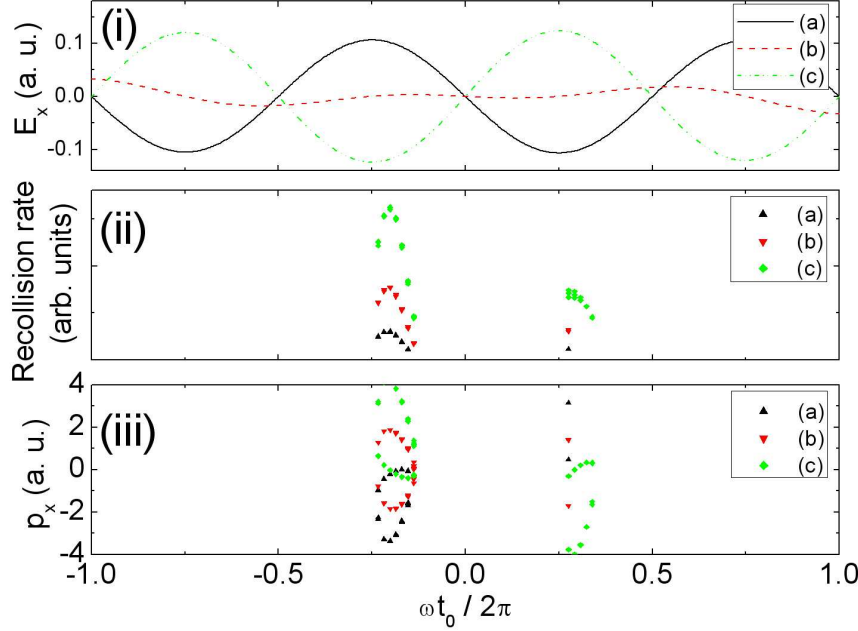


Figure 6. Laser electric field in the x direction (panel (i)), recollision rate (panel (ii)) and the final electron momentum along $p_{1x} = p_{2x} = p_x$ (panel (iii)), as functions of the phase ωt_0 , for a pulse described by Eqs. (3) and (4), with CE phase of 0.5π and three different phase delays of $\omega T_d = 8\pi$, 7π and 6π [tags (a), (b) and (c), respectively]. The remaining parameters are the same as in Fig. 1.

sake of clarity, we are no longer employing the notation $p_{n\parallel}$.

It is found that, actually, the electron momentum distributions evolve gradually from the third quadrant to the first quadrant, with the decrease of the delay phase between 8π and 6π . And interestingly, at a delay phase of 7π , the electron distribution is almost centered at the origin (Fig. 5(c)). This is quite different from the case with a linearly polarized few-cycle pulse, for which the center of the electron momentum distribution is always at nonvanishing momenta and the distributions just “jump” from one quadrant to another. This is due to the fact that, in the linearly-polarized, few-cycle case, the “jump” is caused by a shift in the dominant set of orbits, while, in the present situation, the dominant set of trajectories remains the same. The changes occur in the momentum components in the x direction.

This modification in the most probable momenta is due to the fact that the polarization gate changes direction within this phase-delay interval. In fact, as the x momentum components p_{nx} , ($n = 1, 2$) decrease, there is a corresponding increase in the momentum components p_{ny} , ($n = 1, 2$). This is explicitly shown in the lower panels of Fig. 5, which exhibit exactly the opposite behavior as in the upper panel, i.e., an increase in the peak momenta of the distributions as ωT_d is shifted from 8π to 7π , followed by a decrease when this delay is further shifted to 6π . In fact, while for Figs. 5(f) and 5(j) the distributions exhibit a peak near $p_{1y} = p_{2y} = 0$, in the central

panel [Fig. 5(h)] the absolute value of the peak momentum is near $2\sqrt{U_p}$.

In order to understand this more clearly, we plot in Fig. 6 the laser electric field in the x direction, the recollision rate and the final electron momentum along $p_{1x} = p_{2x} = p_x$ as functions of the phase ωt_0 , for three different delay phases of $\omega T_d = 8\pi, 7\pi$ and 6π . From the upper panel in Fig. 6, one finds that, for $\omega T_d = 7\pi$, the field amplitude in the x direction is very small around the center of the gate, because the two combining field components in x direction are totally out of phase. While for $\omega T_d = 8\pi$ and 6π , the fields have maximal amplitudes but opposite directions due to their relative phase shift of π .

As discussed in section 2, the center of the hypersphere which delimits the momentum distributions in momentum space is determined by the vector potential-component $A_x(t)$ at the instant when the electron recollides. For $\omega T_d = 7\pi$, the amount of momentum the electron acquired from the combined field is thus very small in the x direction. Hence, the classically allowed region is approximately centered at momentum $p_x = 0$, as shown in Fig. 6(iii). For $\omega T_d = 8\pi$ and 6π , the relative shift of 2π in the delay phase results in the inversion of the x-component of the combined field at the very center of the polarization gate. This gives rise to electron emission in the opposite direction, i.e., the electron momentum distribution shifts from the third to the first quadrant.

4. Conclusions

In this work, we have studied laser-induced nonsequential double ionization (NSDI) with a polarization-gated driving pulse. The specific pulse employed here consisted of two few-cycle pulses with opposite circular polarizations and a time delay T_d (for details we refer to [5]). The ellipticity of the combined field is time-dependent and vanishes for $t_0 = 0$. The larger the time delay between both pulses, the steeper the time-dependence in the polarization. We performed such studies within a classical framework, extending the model in Ref. [10, 11, 13] to elliptically polarized fields.

We found that the electron-momentum distributions, as functions of the electron components parallel to the laser-field polarization at the center of the gate, are very much dependent on the delay between the two few-cycle pulses \vec{E}_r and \vec{E}_l composing the polarization-gated pulse. For long delays that are chosen as multiple times of the pulse duration, the distributions are asymmetric and dependent on the CE phase of such pulses. This is similar to the behavior observed for a single linearly polarized, few-cycle driving pulse [10, 11]. As the time delay T_d decreases, this asymmetry fades. We could explain this behavior in terms of trajectories. Below we will summarize the main aspects of this explanation, and also draw a parallel between the present situation and the previously studied case of linearly polarized, few-cycle pulses [10, 11].

For linearly polarized few cycle pulses, the momentum region in which the electron momentum distributions will be concentrated depends on the quasi-static tunneling rate for the first electron and on the momentum region for which NSDI is classically allowed. A large rate and a large momentum region imply that the contributions from a specific set of trajectories to the distributions will be prominent. For very short pulses, there is in general a single set of trajectories that best fulfills such conditions. This set will change with the CE phase. As the pulse length increases, more and more sets of trajectories will lead to prominent contributions, and the asymmetry will fade.

For polarization gated pulses, the most relevant set of orbits will be that closest to the polarization gate, i.e., to the quasi linearly polarized region of the pulse. Indeed,

the first electron will tunnel more efficiently than for the remaining set of orbits. This is due to the fact that the electron velocity components perpendicular to the main polarization axis of the laser field is smallest for the dominant set of orbits.

Apart from that, the first electron will return more easily to the parent ion if it was released near the polarization gate. This will happen for two main reasons. First, the small lateral velocity components will not lead to a significant initial motion in the transverse direction. Second, the electron will propagate in the continuum in a time interval close to the gate. Hence, it will be accelerated in the transverse direction to a lesser extent than for the remaining sets of orbits. This will guarantee an efficient return to the ion.

For an efficient polarization gate, the changes in the driving-field ellipticity within the pulse length are very steep, so that only the orbits close to the gate will contribute significantly to the distributions. In general, this will lead to highly asymmetric electron momentum distributions, concentrated in the momentum region determined by the dominant orbits. This is a similar behavior to that encountered for linearly polarized driving fields, in the sense that, in general, only one set of trajectories dominates the yield.

If the gate, however, is less efficient, the contributions from the other sets of orbits will be increasingly important. Ultimately, this will lead to nearly symmetric electron-momentum distributions. For the specific driving pulse in this work, this effect has been observed by decreasing the delay T_d between the pulses.

In general, the efficient use of polarization gates could tremendously increase the degree of attainable control of strong field ionization dynamics, compared to the commonly used single linearly polarized few-cycle pulse. For the latter, only the scalar properties of laser pulses is used, while a polarization gate can, in principle, as demonstrated in this work, make full use of the flexibility of the vectorial laser field, e.g., the polarization state, as an additional knob, to steer the NSDI dynamics within sub-cycle time resolution.

Acknowledgments

X. Liu acknowledges the financial support from the NNSF of China (No. 10674153) and C.F.M.F from the UK EPSRC (Advanced Fellowship, Grant no. EP/D07309X/1).

- [1] Corkum P B, Burnett N H, and Yvanov M, 1994 *Opt. Lett.* **19** 1870
Dietrich P, Burnett N H, Ivanov M, and Corkum P B, 1994 *Phys. Rev. A* **50** R3585
Ivanov M, Corkum P B, Zuo T, and Bandrauk A, 1995 *Phys. Rev. Lett.* **74** 2933
Antoine P, Milošević D B, L'Huillier A, Gaarde M B, Salières P, and Lewenstein M, 1996 *Phys. Rev. A* **54** R1761
- [2] Mairesse Y, Dudovich N, Levesque J, Ivanov M Yu, Corkum P B and Villeneuve D M, 2008 *New J. Phys.* **10** 025015
- [3] Sola I J, Mével E, Elouga L, Constant E, Strelkov V, Poletto L, Villoresi P, Benedetti E, Caumes J -P, Stagira S, Vozzi C, Sansone G and Nisoli M 2006 *Nature Physics* **2** 318
- [4] Shan B, Ghimire S and Chang Z, 2005 *J. Mod. Opt.* **52** 277
- [5] Chang Z, 2004 *Phys. Rev. A* **70** 043802.
- [6] Sansone G, Benedetti E, Calegari F, Vozzi C, Avaldi L, Flammini R, Poletto L, Villoresi P, Altucci C, Velotta R, Stagira S, Silvestri S D and Nisoli M, 2006 *Science* **314** 443
- [7] Corkum P B, 1993 *Phys. Rev. Lett.* **71** 1994
- [8] Weber Th, Giessen H, Weckenbrock M, Staudte A, Spielberger L, Jagutzki O, Mergel V, Vollmer M, and Dörner R, 2000 *Nature* **405** 658
Feuerstein B, Moshhammer R, Fischer D, Dorn A, Schröter C D, Deipenwisch J, Crespo Lopez-Urrutia J R, Höhr C, Neumayer P, Ullrich J, Rottke H, Trump C, Wittmann M, Korn G and Sandner W, 2001 *Phys. Rev. Lett.* **87** 043003

- [9] Liu X, Rottler H, Eremina E, Sandner W, Goulielmakis E, Keeffe K O, Lezius M, Krausz F, Lindner F, Schätzel M G, Paulus G G and Walther H 2004 *Phys. Rev. Lett.* **92**, 263001
- [10] Liu X, Figueira de Morisson Faria C 2004 *Phys. Rev. Lett.* **92** 133006 .
- [11] Figueira de Morisson Faria C, Liu X, Sanpera A and Lewenstein M, 2004 *Phys. Rev. A* **70** 043406
- [12] Shvetsov-Shilovski N I, Goreslavski S P, Popruzhenko S V, and Becker W, 2008 *Phys. Rev. A* **77** 063405
- [13] Figueira de Morisson Faria C, Schomerus H, Liu X and Becker W, 2004 *Phys. Rev. A* **69** 043405
- [14] Chen J, Liu J, Fu L B, and Zheng W M, 2001 *Phys. Rev. A* **63** 011404(R)
Fu L B, Liu J, Chen J, and Chen S G, 2001 *Phys. Rev. A* **63** 043416
Fu L B, Liu J, and Chen S G, 2002 *Phys. Rev. A* **65** 021406 (R)
Chen J, Liu J, and Zheng W M, 2002 *Phys. Rev. A* **66** 043410
Haan S L, Wheeler P S, Panfili R, and Eberly J H, 2002 *Phys. Rev. A* **66** 061402(R)
Panfili R, Haan S L, and Eberly J H, 2002 *Phys. Rev. Lett.* **89**, 113001
- [15] Liu X, Figueira de Morisson Faria C, Becker W and Corkum P B 2006 *J. Phys. B* **39** L305
- [16] Cavalieri A L, Goulielmakis E, Horvath B, Helm W, Schultze M, Fieß M, Pervak V, Veisz L, Veisz L, Yakovlev V S, Uiberacker M, Apolonski A, Krausz F and Kienberger R 2007 *New J. Phys.* **9** 242
- [17] Keldysh L V, 1964 *Zh. Eksp. Teor. Fiz.* **47** 1945 [1965 *Sov. Phys. JETP* **20** 1307].
- [18] Delone N B and Krainov V P, 1991 *J. Opt. Soc. Am. B* **8** 1207
- [19] de Jesus V L B, Feuerstein B, Zrost K, Fischer D, Rudenko A, Afaneh F, Schröter C D, Moshhammer R and Ullrich J 2004 *J. Phys. B: At. Mol. Opt. Phys.* **37** L161
- [20] Dudovich N, Levesque J, Smirnova O, Zeidler D, Comtois D and Ivanov M Yu, 2006 *Phys. Rev. Lett.* **97** 253903